Chiral knife edge: A simplified rattleback to illustrate spin inversion

Eduardo A. Jagla
Comisión Nacional de Energía Atómica and Instituto Balseiro CNEA, CONICET, UNCUYO Avenida E. Bustillo 9500 S. C. de Bariloche, Argentina

Alberto G. Rojo
Department of Physics, Oakland University, Rochester, Michigan 48309, USA

(Received 24 July 2023; accepted 20 November 2023; published 26 December 2023)

We present the chiral knife edge rattleback, an alternative version of previously presented systems that exhibit spin inversion. We offer a full treatment of the model using qualitative arguments, analytical solutions as well as numerical results. We treat a reduced, one–mode problem which not only contains the essence of the physics of spin inversion, but that also exhibits an unexpected connection to the Chaplygin sleigh, providing insight into the nonholonomic structure of the problem. We also present exact results for the full problem together with estimates of the time between inversions that agree with previous results in the literature.

DOI: 10.1103/PhysRevE.108.064213

I. INTRODUCTION

The rattleback, or *celt*, is a boat-shaped stone (commercially available as a toy) which exhibits unintuitive behavior that at first glance seems to defy the law of conservation of angular momentum. In its usual version it consists of a simple rigid body with a semiellipsoidal bottom and an uneven distribution of mass so that the axes of symmetry of the ellipsoid do not coincide with the principal axes of inertia of the rigid body.

As with a symmetric semiellipsoidal top, the rattleback can oscillate with respect to two horizontal axes in modes usually called "rolling" and "pitching," as shown schematically in Fig. 1. When the rattleback is spun in one direction, it quickly starts to roll up and down while the rotation velocity first decreases, and eventually it changes sign. After a few turns it soon begins pitching until the rotation changes direction again. Were it not for unavoidable mechanical losses, this periodic inversion of the rotation direction would continue indefinitely. The misalignment between the principal axes of inertia of the body and those of the curvature at the contact point (generating a definite *chirality* in the system) couples the spinning motion with the pitching and rolling oscillations. As a result of this misalignment, the frictional contact force creates a torque about the center of mass, causing the top to invert its motion.

Most of previous analyses of the rattleback [1–4] describe the motion by approximating the contact surface of the body as an ellipsoid whose principal axes are rotated with respect to the principal axes of inertia. The equations of motion are then treated in various approximations and solved numerically to illustrate the spin inversion. In this paper we propose an alternative version of the rattleback in the form of a knife edge with hanging masses that can execute the rolling and pitching motion, with the center of mass below the point of contact. We performed some experimental tries with the physical model shown in Fig. 2

Our derivation of the equations of motion is simpler than that of previous treatments, and these equations are even suitable for pedagogical expositions that illuminate the origin of spin inversion. In order to distill the essence of the mechanism of spin inversion, we first treat a simplified model in which we freeze one of the oscillating modes—the single-mode rattleback.

In Sec. II we describe the simplified single-mode case, present a qualitative explanation of its behavior and solve the full non-holonomic equations of motion using a few reasonable approximations. The resulting equations are simple and amenable to a transparent interpretation of the origin of the spin inversion. In addition, we rewrite the equations in terms of the amplitudes of motion of the oscillating and spinning mode, and retrieve by, in our opinion, a more direct and "microscopic" route the equations of motion (restricted to one mode) proposed by Tokieda and collaborators [5,6]. In addition, we find a puzzling and unexpected equivalence of our single-mode rattleback with the Chaplygin sleigh, one of the classic irreversible nonholonomic systems.

In Sec. III we extend the treatment to the knife edge rattleback with two modes. We follow the standard nonholonomic program to obtain analytical expressions for the equations of motion. We also present numerical solutions that show an equivalence with the traditional treatments.

II. SINGLE-MODE KNIFE EDGE RATTLEBACK

The rattleback effect is driven by a shift of the supporting point with the oscillation angles. We first attempt to the simplest description of the phenomenon. We consider a single oscillating mode, which plays the role of either pitching or rolling in the usual nomenclature of the rattleback, coupled to a spin mode and assume that the second oscillating mode is "frozen." Specifically, our model consists of a rigid massless bar—a knife edge of length $2L$—that stays and moves on the (x, y) plane. Two massless segments of length ℓ are attached

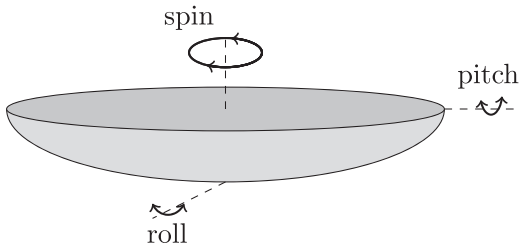

FIG. 1. Scheme of a traditional boat-shaped rattleback. The two oscillations and the rotational degrees of freedom are indicated

to the ends of the bar. These two segments have masses of magnitude $M/2$ attached to their free ends. The set of the three massless segments and the two point masses form a rigid body. The system can spin with angular velocity $\dot{\phi}$ around the z axis and execute small oscillations of angle θ around the vertical, as illustrated in Fig. 3. The choice of this particular geometry is informed by experiments we did with a chiral knife edge that, in order to be stable, requires the center of mass to be below the point of support.

The configuration space of the system is determined by the two angles θ and ϕ, and the position $\mathbf{x}$ of the center of the horizontal bar (point O in Fig. 3) on the x, y plane. To completely define the dynamics of the model, we need to specify the sliding conditions of the horizontal bar on the plane. We will assume that at any moment there is a single contact point $\mathbf{x}_C$ with a nonslip condition between the bar and the plane. The instantaneous zero velocity of the physical contact point is the additional ingredient that completely defines the dynamics. Yet, the nontrivial condition from which the subtle properties of the system will emerge is the change of contact point with the value of θ. We impose that the instantaneous contact point is at a distance $D\theta$ from the center $\mathbf{x}$ of the bar:

$$\mathbf{x}_C = \mathbf{x} + D\theta\hat{\mathbf{u}}_\phi,$$

where $\hat{\mathbf{u}}_\phi$ is a unit vector in the direction of the bar. This prescription, that introduces chirality into the system, will be fully justified within the more complete modeling that

FIG. 2. Chiral rattleback built using a pizza cutter disk as a knife edge. The cylinder is for support only and is kept fixed.

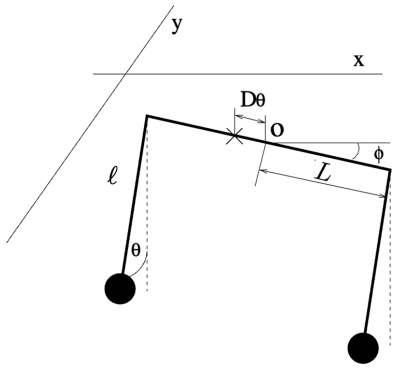

FIG. 3. Sketch of the single-mode rattleback. The horizontal bar lies completely on the x, y plane, at an angle ϕ with respect to $\hat{x}$. The instantaneous contact point (indicated by $\times$ and having zero velocity) is at distance $D\theta$ from the center point O.

includes the two oscillating modes of the system and a more realistic knife edge geometry, to be presented in Sec. III.

The essence of the single-mode system is that there is only one oscillatory degree of freedom (in addition to the unconstrained rotation around $\hat{z}$), so the second oscillation must be frozen, somehow. In Fig. 4 we propose a possible physical realization of the single mode. The (half)-cylindrical shape of the body prevents the rolling oscillation (Fig. 1) to take place. Note that in this case the center of mass of the system is above the contact point.

A. Qualitative explanation of the spin inversion

Consider the case in which $D = 0$, namely, the contact point is always the middle point of the bar. Also, let us take $\dot{\phi} = 0$. Under these conditions all we have is a simple pendulum which, for small values of θ, executes a harmonic motion of the form

$$\theta(t) \propto \cos\omega_0 t. \tag{1}$$

This oscillation does not couple to ϕ. During the oscillation, there is a friction force (provided by the constraint) of the form

$$f(t) \propto \ddot{\theta}(t) \propto -\theta(t) \tag{2}$$

acting at the pendulum's support point, as sketched in Fig. 5(a).

If the contact point changes with θ (i.e., $D \neq 0$), the force $f(t)$ will now be applied at a distance $D\theta$ away from the center O of the bar [Fig. 5(b)]. This force now generates a torque with

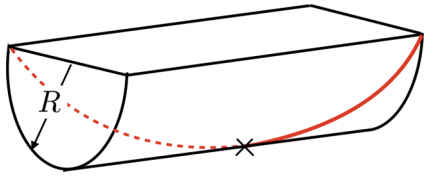

FIG. 4. A possible realization of the single-mode rattleback, consisting of a half-cylinder with a helical knife edge (marked in red). The line of contact of the cylinder with the table is frictionless, with the exception of the point of contact of the knife edge with the table (marked with a cross), which has zero instantaneous velocity.

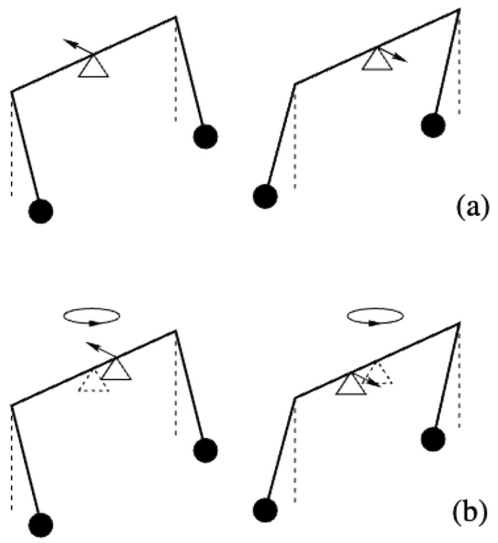

FIG. 5. Origin of the oscillation-spin coupling in the single-mode rattleback. In (a) the supporting point is kept fixed, and the reaction force due to the oscillation (indicated with the arrows) does not generate any torque onto the system. In (b) the supporting point shifts proportionally to θ, and therefore the reaction force produces a torque always with the same orientation.

respect to O, giving rise to an acceleration of ϕ in the form

$$\ddot{\phi} \sim f \times D\theta \sim -D\theta^2. \tag{3}$$

The torque appears in a well-defined direction, independently of the sign of θ, and is proportional to the energy of the oscillatory mode. Note that this fact appeared as a postulate in one of the first full mathematical treatments of the rattleback [7].

This pedagogical exposition of the oscillation-rotation coupling is at the heart of the rattleback effect in more complex setups. Now we proceed to the full analysis of this single-mode rattleback.

B. Full analysis

The unconstrained Lagrangian of the system in Fig. 3 is

$$\mathcal{L} = \tfrac{1}{2}M(\dot{\mathbf{x}}^2 + \ell^2\dot{\theta}^2 + L^2\dot{\phi}^2 + 2\ell\dot{\theta}\dot{\mathbf{x}}\cdot\hat{\mathbf{v}}_\phi) - \tfrac{1}{2}Mg\ell\theta^2,$$

where $\hat{\mathbf{v}}_\phi = (-\sin\phi, \cos\phi)$ is a unit vector perpendicular to the instantaneous direction of the horizontal bar, and ϕ is the angle of the bar with respect to the x axis on the plane of the table.

The two nonholonomic constraints are zero velocity of the point of contact along the direction of the bar (note that the point of contact is at rest with respect to the bar),

$$\hat{\mathbf{u}}_\phi \cdot \dot{\mathbf{x}} = 0, \tag{4}$$

and zero velocity in the direction perpendicular to the bar,

$$\dot{\mathbf{x}} \cdot \hat{\mathbf{v}}_\phi + D\theta\dot{\phi} = 0, \tag{5}$$

with $\hat{\mathbf{u}}_\phi = (\cos\phi, \sin\phi)$ the unit vector in the direction of the bar.

The constraint equations (4) and (5) are linear and can be written in matrix form as $\sum_{j=1}^{2} a_{i,j}(\mathbf{q})\dot{q}_j = 0$, with $i = 1, 2$, and $\mathbf{q}$ the coordinates $(\mathbf{x}, \theta, \phi)$. As is standard in the treatment of nonholonomic systems [8], we impose the constraints in the equations of motion through Lagrange multipliers:

$$\frac{d}{dt}\frac{\partial\mathcal{L}}{\partial\dot{q}_i} - \frac{\partial\mathcal{L}}{\partial q_i} = \sum_{j=1}^{2}\lambda_j a_{j,i}(\mathbf{q}). \tag{6}$$

Our constrained equations have the form

$$ML^2\ddot{\phi} = -M\ell\dot{\theta}\dot{\mathbf{x}}\cdot\hat{\mathbf{u}}_\phi + \lambda_2 D\theta \tag{7a}$$

$$M\left(\ell^2\ddot{\theta} + \ell\frac{d}{dt}\dot{\mathbf{x}}\cdot\hat{\mathbf{v}}_\phi\right) = -Mg\ell\theta \tag{7b}$$

$$M\left(\ddot{\mathbf{x}} + \ell\frac{d}{dt}\dot{\theta}\hat{\mathbf{v}}_\phi\right) = \lambda_2\hat{\mathbf{v}}_\phi + \lambda_1\hat{\mathbf{u}}_\phi. \tag{7c}$$

From Eq. (7c) and using the constraints we obtain

$$\lambda_2 = M(-D(\dot{\phi}\dot{\theta} + \theta\ddot{\phi}) + \ell\ddot{\theta}). \tag{8}$$

Replacing the value of the multiplier in Eq. (7a) we obtain

$$ML^2\ddot{\phi} = \lambda_2 D\theta \simeq MD\theta(-D\dot{\phi}\dot{\theta} + \ell\ddot{\theta}), \tag{9}$$

where we neglected a term $\sim\theta^2\ddot{\phi}$ over $\sim\ddot{\phi}$, an approximation which we will also adopt in what follows.

The equations of motion for θ and ϕ become

$$\ddot{\phi} = \frac{D\ell}{L^2}\theta\ddot{\theta} - \left(\frac{D}{L}\right)^2\theta\dot{\theta}\dot{\phi}, \tag{10a}$$

$$\ddot{\theta} = -\frac{g}{\ell}\theta + \left(\frac{D}{\ell}\right)(\theta\ddot{\phi} + \dot{\theta}\dot{\phi}). \tag{10b}$$

Finally, note that from Eq. (10b) we have

$$\theta\dot{\theta}\dot{\phi} = \frac{\ell}{D}\ddot{\theta}\theta + \frac{g}{D}\theta^2 - \theta^2\ddot{\phi},$$

which when replaced in Eq. (10a) leads to the final form of the equations of motion, and constitutes one of the results of the present paper:

$$\ddot{\phi} = -\frac{gD\ell}{L^2}\theta^2, \tag{11a}$$

$$\ddot{\theta} = -\frac{g}{\ell}\theta + \frac{D}{\ell}\dot{\theta}\dot{\phi}. \tag{11b}$$

The above equations contain the essential elements of spin inversion. Equation (11b) describes a harmonic oscillator of amplitude $\theta(t)$ with a friction term with effective friction coefficient $-\frac{D}{\ell}\dot{\phi}$. This frictional term comprises the back action of the ϕ mode over θ. Equation (11a) corresponds to a torque around the z axis of constant sign, in agreement with the qualitative argument presented in Sec. II A. If we start with $\dot{\phi} > 0$ and θ infinitesimal, the "negative friction" term in Eq. (11b) gives rise to an increase in amplitude of θ and, from Eq. (11a), a simultaneous decrease in the value of $\dot{\phi}$. This decrease is monotonous, as it is proportional to $-\theta^2$. When $\dot{\phi}$ changes sign, the corresponding frictional term gives rise to an attenuation of the amplitude of θ until $\dot{\phi}$ is constant and negative. This behavior is illustrated in Fig. 6 where we show a numerical solution of Eqs. (11).

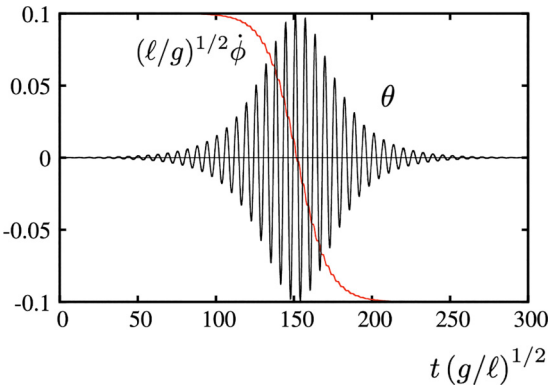

FIG. 6. Numerical solution of the single-mode rattleback of Eqs. (11) illustrating the spin inversion accompanied by an increase and decrease of the amplitude of the oscillating mode. The initial condition has $\dot{\phi} = 0.1\sqrt{g/\ell}$, and θ very small. Other parameters used were $\ell/L = 1$, $D/\ell = 1$.

C. The single-mode rattleback and the Chaplygin sleigh

There is a remarkable formal analogy between the present single-mode rattleback and one of the prototypical nonholonomic mechanical systems—the Chaplygin sleigh [9] shown in Fig. 7.

The analogy emerges when considering the previous equations of the single-mode rattleback in terms of slightly different variables. Let us first define

$$A_\phi = \dot{\phi}.$$

We now separate the motion in the periodic mode as $\theta(t) = A_\theta(t)e^{i\omega t}$. We are interested in a situation in which the "bare" frequency ω of the mode is large, that is,

$$\dot{\phi} \ll \omega = \sqrt{\frac{g}{\ell}},$$

and where $A(t)$ is slowly varying in the timescale of $1/\omega$, that is, $\dot{A} \ll \omega$. In this regime we are safe to make the following approximation for θ^2 (replacing $\cos^2\omega t$ by its mean value $\langle\cos^2\omega t\rangle = 1/2$),

$$\theta^2 \simeq \tfrac{1}{2}A_\theta^2(t),$$

and we are safe to neglect the terms indicated below for the time derivatives of $\theta(t)$:

$$\dot{\theta} = \{\dot{A}_\theta + i\omega A\}e^{i\omega t} \simeq i\omega A_\theta e^{i\omega t}, \tag{12}$$

$$\ddot{\theta} = \{\ddot{A} + 2i\omega\dot{A}_\theta - A_\theta\omega^2\}e^{i\omega t} \simeq \{2i\omega\dot{A}_\theta - A_\theta\omega^2\}e^{i\omega t}. \tag{13}$$

Replacing Eq. (13) in Eq. (11b) we obtain

$$\{2i\omega\dot{A}_\theta - A_\theta\omega^2\}e^{i\omega t} = -A_\theta\omega^2 e^{i\omega t} + \frac{D}{\ell}i\omega A_\theta e^{i\omega t}\dot{\phi}, \tag{14}$$

$$\dot{A}_\theta = \frac{D}{2\ell}A_\theta A_\phi, \tag{15}$$

and therefore we arrive at

$$\dot{A}_\phi = -\frac{gD\ell}{2L^2}A_\theta^2, \tag{16a}$$

$$\dot{A}_\theta = \frac{D}{2\ell}A_\theta A_\phi. \tag{16b}$$

These equations have the same structure as those of the Chaplygin sleigh, provided we identify the variable v (the velocity along the sleigh, or $\dot{\xi}$ in the notation of Fig. 7) with the amplitude $\dot{\phi} = A_\phi$, and the orientation of the sleigh θ with the amplitude of the single oscillatory mode A_θ of the rattleback. In fact, the well-known tendency of the sleigh to convert its rotational energy into a positive value of v corresponds to the property of the single-mode rattleback to harvest the kinetic energy of the oscillation, and transform it into rotational motion around z, with a well-defined chirality. This remarkable analogy provides a different interpretation of the process of spin inversion in the rattleback, as it shares a close formal analogy with the irreversible dynamics of the Chaplygin sleigh. The physical difference rests in the fact that v in the sleigh corresponds to a linear velocity, whereas A_ϕ corresponds to an angular velocity.

As with the sleigh [8], Eq. (16b) has a family of equilibria (i.e., points at which the right-hand side vanishes) given by $A_\theta = 0, A_\phi \neq 0$. Linearizing about any of these equilibria, one finds a zero eigenvalue together with a negative eigenvalue if $A_\phi > 0$ (the stable case) and a positive eigenvalue if $A_\phi < 0$ (the unstable case). The solution curves are ellipses in the A_θ, A_ϕ plane, as shown in Fig. 8.

The time dependence of A_θ, A_ϕ can be fully worked out, and the final expressions are

$$A_\phi = A_0 \tanh\left(\frac{A_0 Dt}{2\ell}\right), \tag{17a}$$

$$A_\theta = \frac{A_0 L}{\ell\sqrt{g}}\,\mathrm{sech}\left(\frac{A_0 Dt}{2\ell}\right), \tag{17b}$$

where A_0 is the asymptotic value ($t \to \pm\infty$) of A_ϕ. In Fig. 9 we show the agreement between these solutions and the full solution in Fig. 6.

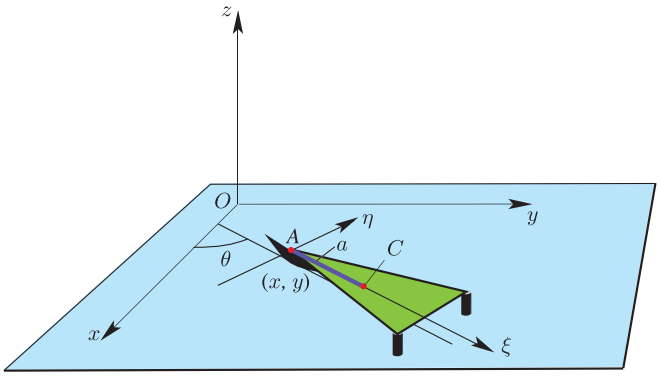

FIG. 7. The Chaplygin sleigh consists of a rigid body supported on a horizontal plane at three points, two of which slide freely without friction while the third (point A) is a knife edge, a constraint that allows no motion perpendicular to its edge. (Picture used with permission from Anthony Bloch's book [8].)

III. TWO-MODE KNIFE EDGE RATTLEBACK

The single-mode rattleback we discussed in the previous section sheds light on the origin of the coupling mechanism between oscillation and (chiral) rotation. Yet it was presented

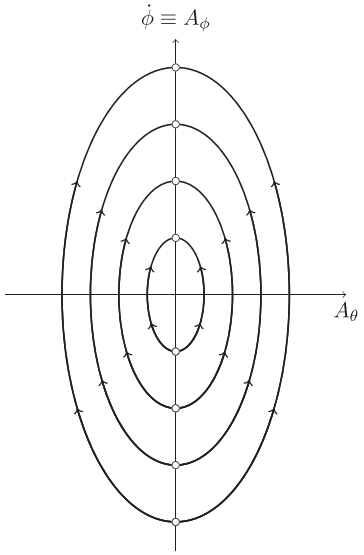

FIG. 8. Phase portrait of the motion amplitudes of the single-mode rattleback.

with a "prescription" for the shift of the contact point. It is important to check if this mechanism, or a similar one, can be implemented in a well-defined mechanical system that includes both the pitching and rolling modes. We show here that a fully consistent two-mode rattleback can be constructed starting from the ideas of the previous section.

We use a similar geometry of two masses hanging from the ends of a bar with an inverted "U" form. However, the horizontal part of the bar is modified to set the contact point as sketched in Fig. 10. The central portion of the bar has a semicircular profile of radius D. The plane of the circle is perpendicular to the horizontal plane and forms an angle α with the bar, as indicated in Fig. 10(b).

The configuration of the system is determined by two (small) oscillation angles θ_1 and θ_2, the rotation angle ϕ around $\hat{z}$, and the position $\mathbf{x}$ of the middle point of the knife edge. The unconstrained Lagrangian of the system can thus be written as

$$\mathcal{L} = \tfrac{1}{2}M\big\{\dot{\mathbf{x}}^2 + (L^2+\ell^2)\dot{\theta}_2^2 + \ell^2\dot{\theta}_1^2 + L^2\dot{\phi}^2 + 2\ell\dot{\mathbf{x}}\cdot(\dot{\theta}_1\hat{\mathbf{v}}_\phi - \dot{\theta}_2\hat{\mathbf{u}}_\phi)\big\} - \tfrac{1}{2}Mg\ell\big(\theta_1^2+\theta_2^2\big).$$

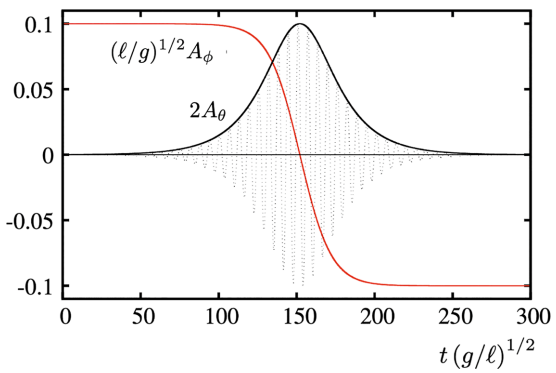

FIG. 9. Analytical solutions [Eqs. (17)] of the amplitude equations (16) for $A_0 = 0.1\sqrt{g/l}$, $\ell/L = 1$, $D/\ell = 1$. In dotted lines we also plot the full solution for θ (Fig. 6) for comparison.

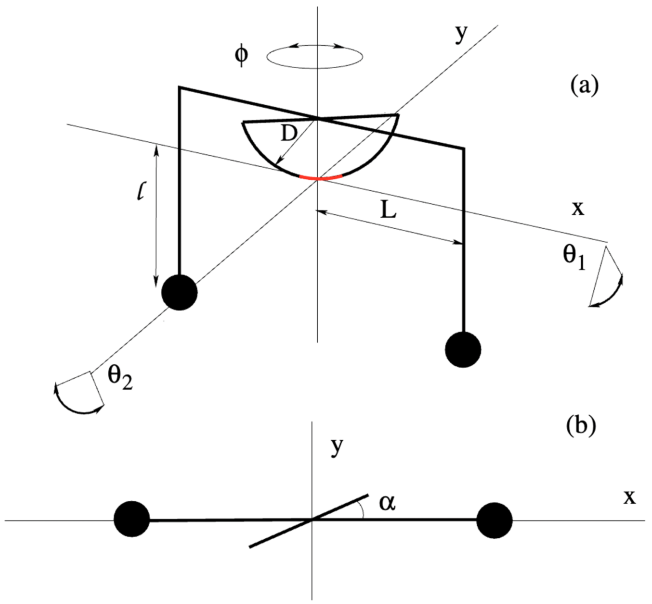

FIG. 10. (a) Sketch of the knife edge, two-mode rattleback. The disk, bars, and masses define a single rigid body. The basic oscillation (θ_1, θ_2) and rotation ϕ modes are indicated. The red part of the disk qualitatively indicates the possible contact points depending of the values of θ_1 and θ_2. (b) Upper view, indicating the definition of the chiral angle α.

The contact point with the supporting surface is the instantaneous lowest point of the circle, and the constraint is that this physical point must has zero velocity. This leads to the following constraints:

$$\dot{\mathbf{x}}\cdot\hat{\mathbf{u}}_\alpha = 0 \tag{18a}$$

$$D\theta_\alpha\dot{\phi} + \dot{\mathbf{x}}\cdot\hat{\mathbf{v}}_\alpha = 0, \tag{18b}$$

where we have defined $\theta_\alpha = (\theta_2\cos\alpha - \theta_1\sin\alpha)$, and $\hat{\mathbf{u}}_\alpha$, $\hat{\mathbf{v}}_\alpha$ are horizontal unitary vectors along and perpendicular to the plane of the circle. From here, the dynamical equations follow:

$$ML^2\ddot{\phi} = -M\ell\dot{\mathbf{x}}\cdot(\dot{\theta}_1\hat{\mathbf{u}}_\phi + \dot{\theta}_2\hat{\mathbf{v}}_\phi) + \lambda_2 D\theta_\alpha \tag{19a}$$

$$M\left(\ell^2\ddot{\theta}_1 + \ell\frac{d}{dt}\dot{\mathbf{x}}\cdot\hat{\mathbf{v}}_\phi\right) = -Mg\ell\theta_1 \tag{19b}$$

$$M\left((\ell^2+L^2)\ddot{\theta}_2 - \ell\frac{d}{dt}\dot{\mathbf{x}}\cdot\hat{\mathbf{u}}_\phi\right) = -Mg\ell\theta_2 \tag{19c}$$

$$M\left(\ddot{\mathbf{x}} + \ell\frac{d}{dt}\big(\dot{\theta}_1\hat{\mathbf{v}}_\phi - \dot{\theta}_2\hat{\mathbf{u}}_\phi\big)\right) = \lambda_2\hat{\mathbf{v}}_\alpha + \lambda_1\hat{\mathbf{u}}_\alpha. \tag{19d}$$

These equations, along with the constraints [Eqs. (18)], enable us to derive the equations of motion in a simplified form by neglecting small terms, as we did previously:

$$\ell^2\ddot{\theta}_1 = -g\ell\theta_1 + D\ell\dot{\theta}_\alpha\dot{\phi}\cos\alpha \tag{20a}$$

$$(\ell^2+L^2)\ddot{\theta}_2 = -g\ell\theta_2 + D\ell\dot{\theta}_\alpha\dot{\phi}\sin\alpha \tag{20b}$$

$$L^2\ddot{\phi} = -D^2\theta_\alpha\dot{\theta}_\alpha\dot{\phi} + \ell D\theta_\alpha(\ddot{\theta}_1\cos\alpha + \ddot{\theta}_2\sin\alpha). \tag{20c}$$

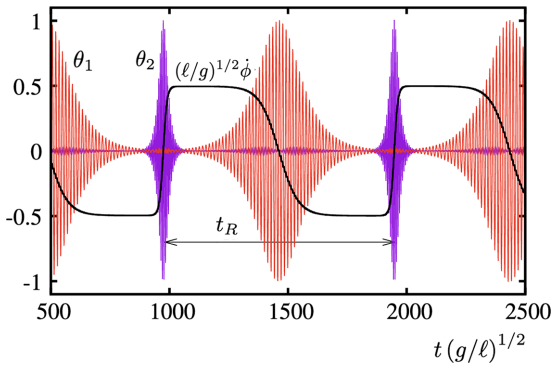

FIG. 11. Numerical solutions of Eqs. (20) with parameters $\ell/L = 1/2$, $D/\ell = 1/2$, $\alpha = \pi/4$. Note the periodic reversal of $\dot{\phi}$, driven alternatively by the activation of the θ_1 and θ_2 modes. The reversal time t_R is indicated.

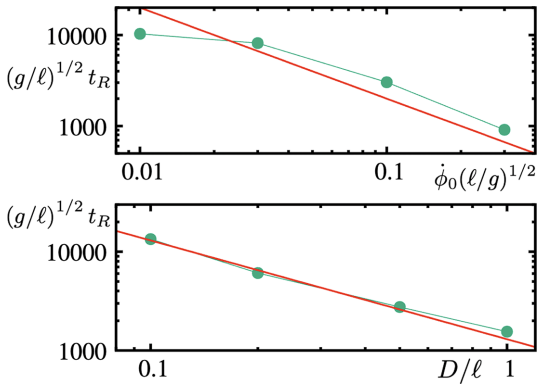

FIG. 12. Numerical results for the inversion time t_R (see Fig. 11) as a function of $\dot{\phi}_0$ for $D/\ell = 1/2$ (a), and as a function of D/ℓ for $\dot{\phi}_0 = 0.1\sqrt{g/\ell}$ (b). In both cases $\ell/L = 1/2$. The straight lines depict a power law with exponent -1, that is, in both cases the expected result for Eq. (22).

These equations are the generalization of those of the previous section for the single-mode model. Note the similarity in the structure. Variables θ_1 and θ_2 are oscillation modes that get an effective friction term proportional to $\dot{\phi}$, which can be positive or negative. In turn, the variable ϕ gets an acceleration that depends quadratically on the θ variables. Note also that there are terms that are proportional to the product $\theta_1\theta_2$ originating in the nonzero chiral angle α. A qualitatively similar set of equations has been derived by Tokieda and collaborators [5,6] using a heuristic approach for the boat-shaped rattleback. We show in Fig. 11 a numerical solution of Eqs. (20) with an initial condition having a finite value of $\dot{\phi}$, and infinitesimal values of θ_1 and/or θ_2 (to avoid remaining at an unstable fixed point). From this initial condition the model evolves by periodically reverting the sign of $\dot{\phi}$ by coupling it alternatively to the oscillation modes. In this way, compared to the single-mode system, there is no longer a systematic tendency to rotate in a single direction but an alternation between rotation in both senses. In the long run, the average value of $\dot{\phi}$ is zero. In addition, in the Supplemental Material [10] a video of our realization of Fig. 2 is presented.

At this point, the following comment is important. We have completely neglected energy dissipation in the problem. In fact, the nonholonomic constraint is nondissipative, as the velocity of the contact point is always zero. This is an ideal situation that can only be approximately satisfied in a real situation. In the case in which some dissipation is included, the rattleback comes to complete stop eventually. It is interesting to note that most common plastic toy rattlebacks display only one of the two possible inversions and a preferred direction of rotation. This is related to the amount of energy dissipation in them that prevents the amplitude increase of the second oscillation mode. In some sense, these toys are dissipation-induced single-mode rattlebacks.

A. Time between spin reversals

A natural question in the rattleback dynamics concerns the time elapsed between spin reversals. A qualitative understanding can be gained from Eqs. (11) and (17). Note from Eqs. (11) that the initial conditions $\theta(0) = \dot{\theta}(0) = 0$ and $\dot{\phi}(0) = \dot{\phi}_0$ constitute an unstable situation for which $\theta(t) = 0$ and $\dot{\phi}(t) = \dot{\phi}_0$. In order for the spin reversal to take place, we need an initial condition $\theta(0) \neq 0$. Now, from Eq. (17b) we see that the time t_0 for θ to increase from a small value $\theta_0 \ll 1$ to its maximum $\theta_{\max}$ is given by

$$t_0 \simeq \frac{1}{\dot{\phi}_0}\frac{\ell}{D}\ln\left(\frac{\theta_0}{\theta_{\max}}\right). \tag{21}$$

In fact, t_R will be $\sim t_0$, if we consider that θ_0 in Eq. (21) is the background value of the inactive mode, at the maximum amplitude of the active mode driving the inversion. Essentially, this is to say that

$$t_R \simeq \frac{1}{\dot{\phi}_0}\frac{\ell}{D} \tag{22}$$

up to a factor that depends weakly (logarithmically) on the parameters of the model and initial conditions chosen. Equation (22) is in agreement with Eq. (46') in Garcia and Hubbard's treatment [7], as well as with Kondo and Nakanishi's paper [11]. We can use this expression to estimate the reversal time t_R in the two-mode case, as defined in Fig. 11. We have done a few simulations to check this expression. In Fig. 12 we show the numerically determined value of t_R for different parameters, showing an overall good agreement to expression (22).

IV. CONCLUSIONS

We presented the chiral knife edge as a model for a rattleback and showed a full treatment of the model using qualitative arguments, and analytical as well as numerical solution of the nonholonomic equations. We first concentrated on a reduced, one-mode problem which contains the essence of the physics of spin inversion. In short, a harmonic oscillation $\theta(t)$ requires a restoring force $f \sim \ddot{\theta}(t) \sim -\theta(t)$. Now, the crucial ingredient of the rattleback is the shift of the contact point from its average positions by an amount $\sim\theta$. Therefore the restoring force generates a torque around $\hat{z}$ of value $\sim\theta^2(t)$ that drives spinning in a well-defined direction.

In the single-mode rattleback, chirality is established by the sign of the displacement of the contact point in relation

with the displacement of the oscillating coordinate. Chirality emerges as different points in configuration space, and their image on a plane mirror cannot be brought to coincide with themselves. This translates into spinning in one preferred sense of rotation. If the initial condition corresponds already to a spin rotation in the preferred direction, the oscillating mode is not excited and spin inversion does not take place. Our treatment vis a vis the analogy with the Chaplygin sleigh shows that the two-mode knife edge rattleback can be assimilated to two dynamically coupled single modes with opposite chiralities. The combined dynamics of the complete system gives rise, in the nondissipative case treated in our paper, to an indefinite sequence of spin inversions.

In addition, we presented an unexpected connection between the single-mode knife edge and the Chaplygin sleigh, a prototypical nonholonomic system. We also presented numerical results for the two-mode knife edge that illustrate spin inversion in both directions. Finally, we presented a qualitative treatment of the time between inversions that agrees with previous results in the literature. We think the paper offers insight on the dynamics of the rattleback, and we plan to explore further consequences in a forthcoming work.

ACKNOWLEDGMENTS

We thank Anthony Bloch and Alfredo Caro for useful comments on the manuscript.

[1] G. T. Walker, On a dynamical top, Q. J. Pure Appl. Math. **28**, 175 (1896).
[2] H. Bondi, The rigid body dynamics of unidirectional spin, Proc. R. Soc. London, Ser. A **405**, 265 (1986).
[3] W. Case and S. Jalal, The rattleback revisited, Am. J. Phys. **82**, 654 (2014).
[4] J. Walker, The mysterious "rattleback": A stone that spins in one direction and then reverses, Sci. Am. **241**, 172 (1979).
[5] H. K. Moffatt and T. Tokieda, Celt reversals: A prototype of chiral dynamics, Proc. R. Soc. Edinb. A: Math. **138**, 361 (2008).
[6] Z. Yoshida, T. Tokieda and P. J. Morrison, Rattleback: A model of how geometric singularity induces dynamic chirality, Phys. Lett. A **381**, 2772 (2017).
[7] A. Garcia and M. Hubbard, Spin reversal of the rattleback: Theory and experiment, Proc. R. Soc. London, Ser. A **418**, 165 (1988).
[8] A. M. Bloch, *Nonholonomic Mechanics* (Springer, New York, 2003).
[9] S. A. Chaplygin, On the theory of motion of nonholonomic systems. The reducing-multiplier theorem, Regul. Chaot. Dyn. **13**, 369 (2008); see also Mat. Sb. **28**, 303 (1912).
[10] See Supplemental Material at http://link.aps.org/supplemental/10.1103/PhysRevE.108.064213 for a video of our setup of Fig. 2 where several inversions can be observed. The video was sped up four times for clarity.
[11] Y. Kondo and H. Nakanishi, Rattleback dynamics and its reversal time of rotation, Phys. Rev. E **95**, 062207 (2017).